Geochemistry Geophysics Geosystems G3

Article
Volume 14, Number 5
6 May 2013
doi:10.1002/ggge.20104
ISSN: 1525-2027

Published by AGU and the Geochemical Society

In situ redeposition of trace metals mobilized by CO_2-charged brines

M. Wigley
Department of Earth Sciences, University of Cambridge, Downing Street, Cambridge, CB2 3EQ, UK (mmw36@cam.ac.uk)

N. Kampman
Department of Earth Sciences, University of Cambridge, Cambridge, UK

H. J. Chapman
Department of Earth Sciences, University of Cambridge, Cambridge, UK

B. Dubacq
Now at UPMC Univ. Paris 06, ISTEP, Paris, France
Also at CNRS, ISTEP, Paris, France

M. J. Bickle
Department of Earth Sciences, University of Cambridge, Cambridge, UK

[1] Mobilization of contaminants by CO_2-charged brines is one concern relating to injection of CO_2 as part of carbon capture and storage projects. This study monitors the mobility of trace metals in an exhumed CO_2-charged aquifer near the town of Green River, Utah (USA), where CO_2-charged brines have bleached red sandstones, and concentrated trace metals at the bleaching reaction front. Mass balance calculations on the trace metal enrichments are used to calculate time-integrated fluid fluxes and show that a significant fraction of the metals mobilized by the CO_2-rich brines are redeposited locally. A sequential extraction procedure on metal-enriched samples shows that these metals are incorporated into secondary carbonate and oxide phases which have been shown to grow at the CO_2-promoted bleaching reaction front. We argue that while CO_2-charged brines are capable of mobilizing trace metals, local metal redeposition implies that the potential for contamination of overlying freshwater aquifers is low.

Components: 6,100 words, 7 figures, 2 tables.

Keywords: CO2; Trace metals; contamination; Green River.

Index Terms: 1065 Geochemistry: Major and trace element geochemistry; 1834 Hydrology: Human impacts.

Received 25 September 2012; **Revised** 7 February 2013; **Accepted** 24 February 2013; **Published** 6 May 2013.

Wigley, M., N. Kampman, H. J. Chapman, B. Dubacq, and M. J. Bickle (2013), In situ redeposition of trace metals mobilized by CO_2-charged brines, *Geochem. Geophys. Geosyst.*, *14*, 1321–1332, doi:10.1002/ggge.20104.

1. Introduction

[2] Geological CO_2 sequestration is proposed as one method for mitigating the effects of fossil fuel burning on global climate [e.g., *IPCC*, 2007]. One of the outstanding scientific questions relates to the potential for injected CO_2 to leak and contaminate overlying freshwater aquifers [*Gale*, 2004; *Smyth et al.*, 2009]. CO_2, injected into geological formations in a gaseous or supercritical state, is likely to dissolve into formation fluids at the gas-water interface, forming acid brines [*Bickle*, 2009; *Dubacq et al.*, 2012]. These brines can mobilize trace metals via desorption of metals bound to mineral surfaces, or by dissolution of trace metal-bearing phases [*Bradl*, 2004; *Yin et al.*, 1996]. If these brines were to migrate into overlying freshwater aquifers, then there is concern that drinking water supplies could be affected. Models [*Wilkin and DiGiulio*, 2010; *Zheng et al.*, 2009] and experiments [*Little and Jackson*, 2010; *Lu et al.*, 2010] have shown that CO_2 can mobilize trace metals; however, field experiments have not shown hazardous levels of contamination [*Keating et al.*, 2010; *Kharaka et al.*, 2010]. Of critical importance is whether the mobilized metals remain in solution or are redeposited locally.

[3] CO_2 has been escaping along the Little Grand Wash and Salt Wash grabens for at least 400,000 years, based on U-Th dating of surface carbonate deposits. [*Kampman et al.*, 2012; *Dockrill and Shipton*, 2010]. Near the town of Green River, Utah, the red-bed Entrada sandstone, exposed by the Salt Wash graben, exhibits spectacular bleaching in which hematite grain coatings are removed and trace metals released from the grain coatings are concentrated at the bleaching reaction front (Figure 1). *Wigley et al.* [2012] argue that the bleaching results from inputs of CO_2-charged brines along the Salt Wash fault, distinguishing the site from hydrocarbon-related bleached sandstones elsewhere on the Colorado Plateau [*Wigley et al.*, 2012; *Loope et al.*, 2010; *Beitler et al.*, 2005, 2003; *Garden et al.*, 2001; *Chan et al.*, 2000]. The CO_2-promoted reaction fronts are used as an analogue for processes occurring where CO_2 leaks from injection sites into overlying aquifers. Here we quantify trace metal enrichments and corresponding time-integrated fluid fluxes [*Bickle and Baker*, 1990] at the bleaching reaction fronts, and use these to calculate the fraction of mobilized metals which have been redeposited. This allows an estimate to be made of the concentration of metals in the solution leaving the CO_2-promoted reaction front.

1.1. Green River Natural Analogue Site

[4] Within the field area, the Jurassic Entrada sandstone is a well-sorted sediment of uniform grain size and mineralogy. Regional burial diagenesis includes the development of Fe-oxide grain coatings [*Cullers*, 1995; *Trimble*, 1978], giving the rock its red color. Along the axis of the Green River anticline, the Entrada sandstone has been bleached by diagenetic fluids which have dissolved the Fe-oxide grain coatings [*Wigley et al.*, 2012]. Bleaching occurs at the base of the formation in a broad domal structure and exposed over a 1–2 km east-west section along the Salt Wash graben (Figure 2a).

[5] Bleaching of red bed sandstones is a common worldwide occurrence, with the bleaching being a result of acid-reductive dissolution of hematite grain coatings, and mobilization of otherwise insoluble Fe^{+3} to soluble Fe^{+2}. Such fluid-rock reaction may be promoted by a wide range of common volatile species (CH_4, CO_2, H_2S, hydrocarbons, and organic acids) present in geological fluids that modify fluid Eh-pH. Several lines of evidence suggest that the fluid causing the bleaching of the Entrada sandstone in the Salt Wash graben was a CO_2-charged brine with minor methane.

[6] Calcite cements and veins associated with the Green River bleaching have a heavier $\delta^{13}C$ than hydrocarbon-related bleaching, consistent with deposition from isotopically heavy C-rich fluids, similar to those in the modern, actively leaking CO_2 system at Green River that underlies the study site [*Assayag et al.*, 2009; *Kampman et al.*, 2009], but inconsistent with isotopically light methane-saturated fluids. Mobilization of low pH-soluble trace metals is inconsistent with methane-rich fluids which have pH $\approx$7.6 when saturated with Fe-oxides (Figure S1 in the supporting information).[1] Regionally, such bleaching is typically localized to structural highs, implicating a low density methane-saturated bleaching fluid. At Green River, bleaching is restricted to the base of the formation, and the morphology of bleached zone is consistent with the flow of a dense fluid as a gravity current, discrediting the role of buoyant methane-saturated bleaching fluids. If the bleaching fluids contained significant H_2S, then hematite would be immediately reprecipitated in situ as pyrite and would not

[1] All supporting information may be found in the online version of this article.

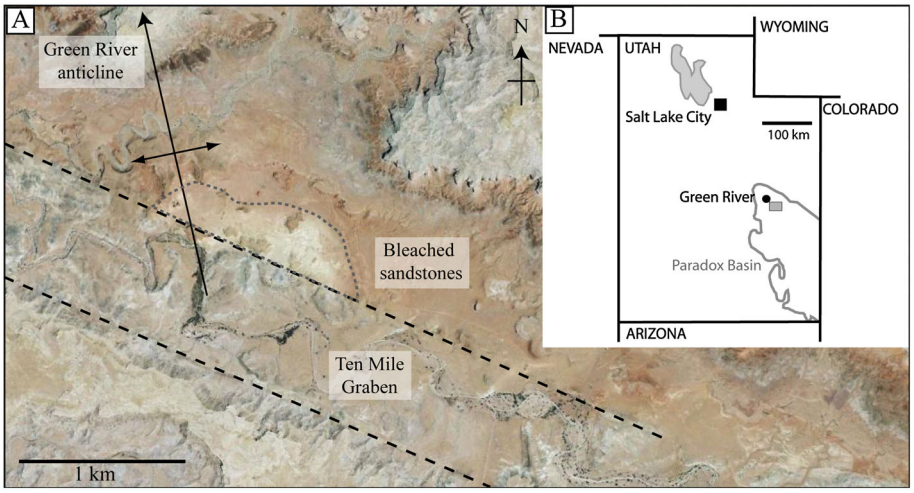

Figure 1. (A) Google earth image of the area of bleached sandstones near the town of Green River, Utah. Dotted gray line shows the extent of the bleaching. Black dashed lines show faults, and solid black arrows mark the Green River anticline. (B) Map of Utah describing the location of the field area. Grey rectangle shows the area in Figure 1A.

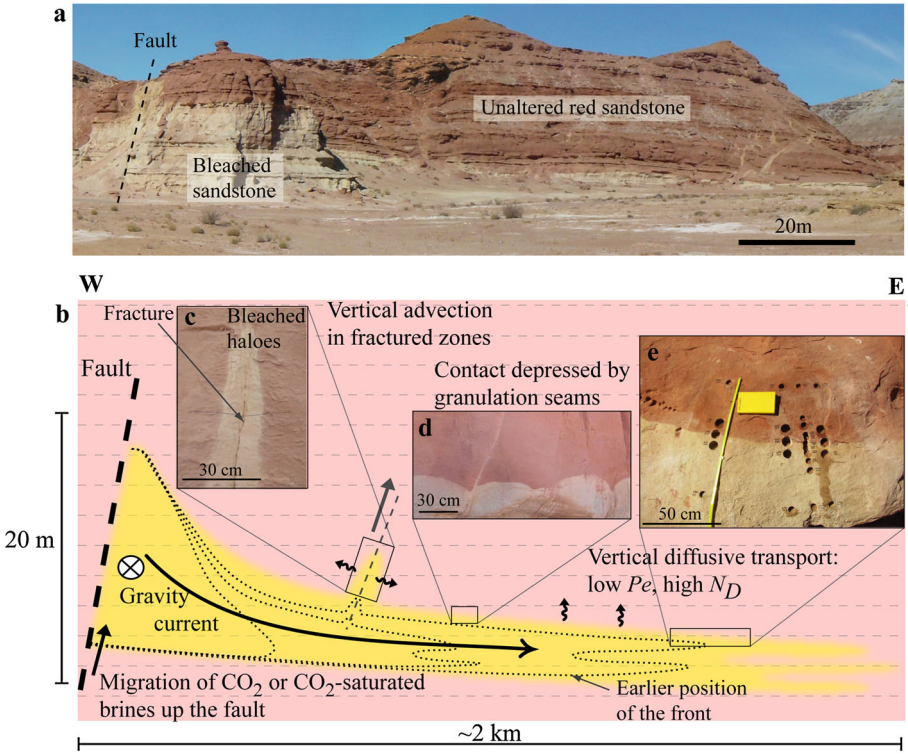

Figure 2. Illustration and outcrop photos of the exhumed CO_2 reservoir. (a) Bleaching at the crest of the anticline, facing north. (b) Schematic development of bleached sandstone (yellow) in original sandstones (red). CO_2 (or CO_2-rich brine) migrated into the formation near the crest of the Green River anticline along faults and flowed laterally as a gravity current. A CO_2-promoted bleaching front (dotted lines) propagated laterally by advection and vertically by diffusion. (d) The preserved reaction front is subhorizontal and exhibits cuspate regions associated with open fractures and granulation seams. (c) Bleached halos develop around vertical fractures. (e) Sampling across subhorizontal reaction fronts.

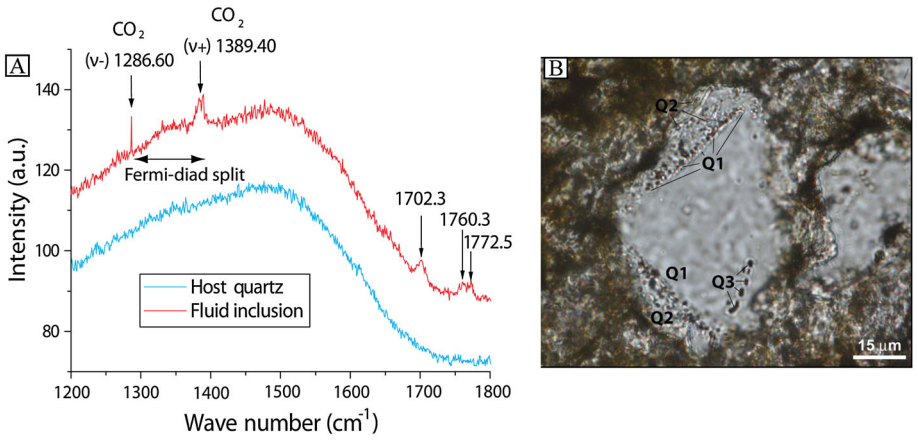

Figure 3. (A) Close up of the region 1200–1800 cm^{-1} for the Raman spectra of the host and the vapor phase of a fluid inclusion in a quartz overgrowth from bleached Entrada sandstone. The CO_2 peaks are marked, along with the Fremi-diad split which is used to calculate a range in CO_2 partial pressures in the bleaching fluid. (B) Plane polarized light image of fluid inclusions hosted in a quartz overgrowth from bleached sandstones.

result in the observed Fe depletion. While some pyrite is observed in fractures, the lack of pyrite (or its Fe-bearing weathering products) throughout the bleached sandstones precludes involvement of significant H_2S.

[7] Microthermometry of single-phase aqueous and two-phase liquid-vapor fluid inclusions hosted in quartz overgrowths and gypsum, petrographically linked to the bleaching, suggests that the bleaching fluid was a low temperature (≈ 27°C) brine (salinity 2.5–7 wt%) [*Wigley et al.*, 2012]. Raman spectroscopic analysis of successfully targeted vapor bubbles reveals gas-phase compositions dominated by CO_2, with minor methane (11–27 vol%) present in three inclusions (Figure 3) [*Wigley et al.*, 2012]. The presence of a free-phase CO_2 bubble suggests the aqueous phase is saturated with CO_2 at the inclusion pressure. The magnitude of the Fermi-diad separation in the Raman spectra of CO_2 is sensitive to the CO_2 density, and this separation has been experimentally calibrated for CO_2 density in the vapor phase, for gaseous CO_2 to liquid CO_2, in the density range of 0.01–1.20 g/cm^3 [*Rosso and Bodnar*, 1995]. Similarly, the Raman peak position of the symmetric C–H stretching mode in CH_4 is dependent on pressure, in CH_4 bearing inclusions [*Lu et al.*, 2007]. Measurements of the Fermi-diad separation in CO_2 spectra reveals CO_2 densities of 0.04–0.09 ±0.02 g/cm^3 which equates to CO_2 pressures of 2.28–4.56 ±1.03 MPa and formation depths of 202–413 ±97 m, assuming hydrostatic pressures. Inclusion pressures based on Raman peak position in CH_4 bearing inclusions [*Lu et al.*, 2007] reveal inclusion pressures of 2.59–3.98 ±1.34 MPa. At these inclusion, pressures dissolved CO_2 concentrations in equilibrium with a CO_2 vapor phase are 0.65–1.30 mol/L, based on the solubility models of *Duan et al.* [2006]. Based on burial curves for the Entrada Sandstone in the area surrounding Green River [*Nuccio*, 2000], modified for local variations in burial depth due to the structural high formed by the Green River anticline, the interval from which these samples were taken passed through the burial depth range 200–400 ±97 m between 2.1 and 5.5 ±1.5 Ma, and this gives an approximate age of the bleaching event.

[8] The upper bleached-red contact is sharp and subhorizontal except in regions of fractures and granulation seams, where differences in porosity and tortuosity enhance or retard vertical transport of the reaction front, respectively (Figures 2b–2c). To the east, the bleached zone terminates as a series of meter scale fingers into red sandstones, while the western extent is not exposed. It is thought that the CO_2-rich brine migrated as a gravity current, with the main components of flow to the east, down dip and in the direction of regional groundwater flow [*Kampman et al.*, 2009], with vertical transport dominated by diffusion except in areas containing faults and open fractures (Figure 2b) [*Wigley et al.* 2012].

[9] The contact between bleached and unbleached sandstone is characterized by stepped profiles in bulk rock Fe-concentration, hematite and K-feldspar abundances, which occur over 10–15 cm, and demarc the final position of the acid-reductive

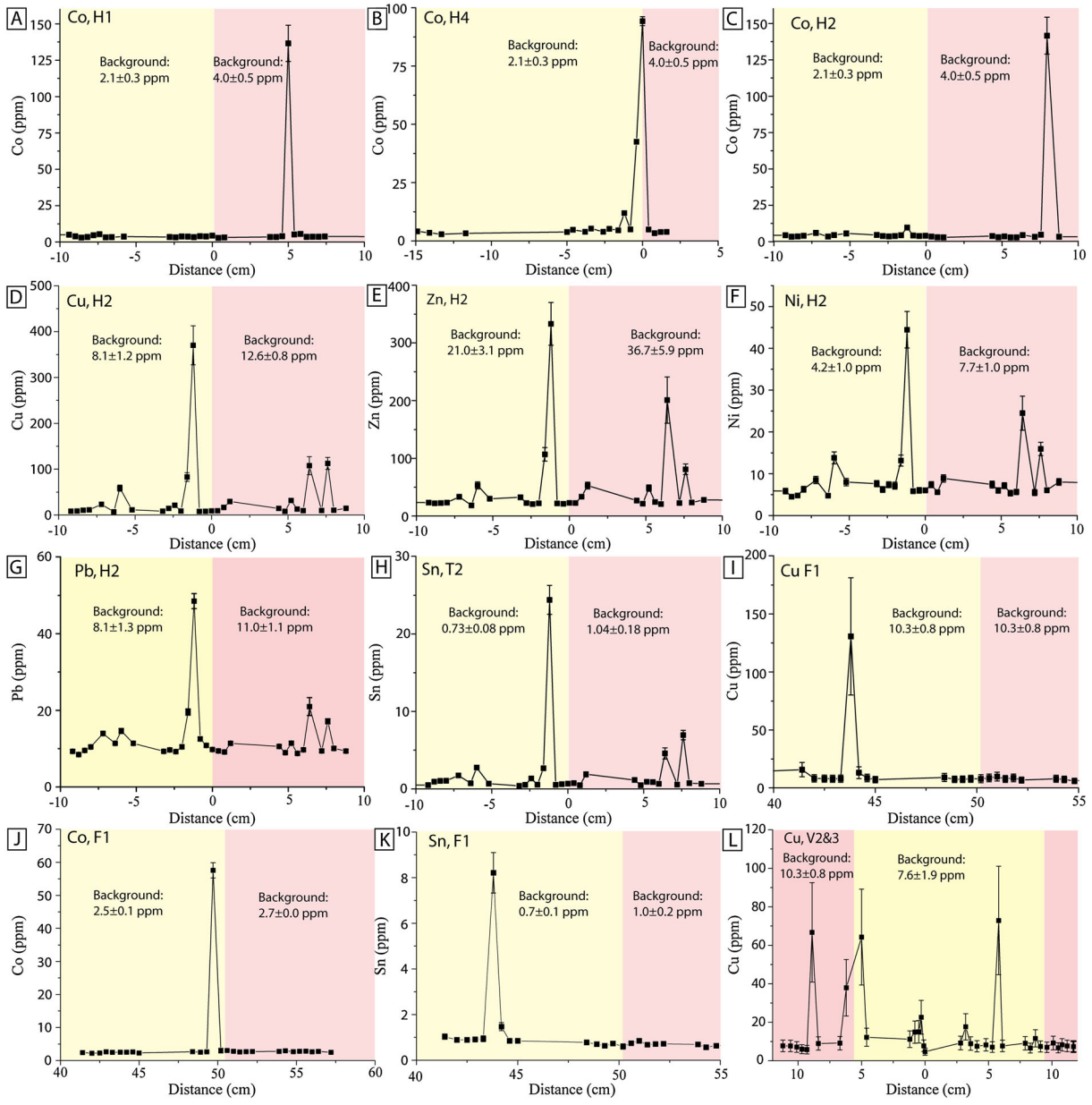

Figure 4. (A–I) Concentration profiles for selected metals across horizontal reaction fronts (distances from the red-bleached transition) and (J–L) fracture-associated reaction fronts (distances from the core of the fracture). Red color denotes unaltered rock, yellow is bleached sandstone. (A–C) Cobalt from transects H1, H4, and H2 showing systematic enrichment within 10 cm of the bleaching reaction front. (C–H) Enrichments in metals along profile H2; (D) Cu, (E) Zn, (F) Ni, (G) Pb, (H) Sn. (I–L) Enrichments across fracture-associated bleaching reaction fronts. (I) Cu, F1; (J) Co, F1; (K) Sn, F1; (L) Cu, F2 and F3. Background concentrations in red and bleached rock are indicated. Error bars show 2σ propagated uncertainties including recovery relative to U.S. Geological Survey (USGS) standard Sco-1, repeat averages, and instrument uncertainties. Raw data and sampling localities are given in Tables S3 and S4.

front. A fine intergrowth of oxide and carbonate is deposited in a 2–3 cm region spanning the reaction front [*Wigley et al.*, 2012]. Bulk rock trace metal enrichments occur systematically in a narrow zone within 5–10 cm of the upper subhorizontal contact (Figure 4a–4h), due to release of trace metals as grain coating Fe-oxides were dissolved, with subsequent redeposition at the reaction front [*Wigley et al.*, 2012]. The enriched metals are characteristic in having high solubilities at low pH [e.g., *Benjamin and Leckie*, 1981], and this mobilization-redeposition is thought to be fundamentally driven

by acid-reductive dissolution of the Fe-oxide grain coatings at low pH, with subsequent transport of the trace metals in solution and redeposition at the reaction front as pH rises due to a combination of pH buffering silicate dissolution reactions and secondary mineralization. The scale of enrichments is determined by the volume of fluid that interacted with the reaction front, which had previously reacted with unaltered rock.

[10] Bleaching also occurs around open fractures (Figure 2c), which are mineralized with carbonate and Fe-oxides, and exhibits the same geochemical and petrological signatures as the subhorizontal bleaching contacts, indicating a common parent fluid and continuity in reactive-transport processes. The fracture-associated bleaching reaction front initiated at the plane of the fracture and migrated laterally by diffusion and advection of the fluid. The asymmetry of the bleached halos is due to the transport away from the fractures being imposed on unidirectional horizontal regional flow in the aquifer [*Wigley et al.*, 2013]. Spikes in trace-metal concentration are observed within 5–10 cm of the red-bleached transition adjacent to the fractures (Figures 4i–4l), similar to those across subhorizontal contacts. These are assumed to be related to deposition of metals released by the bleaching reaction front as it propagates from the fracture, in addition to any metals present in the bleaching fluid entering the fracture, due to the increase in pH across the reaction front.

[11] Key questions include the following: (1) What was the original distribution of the metals? (2) How, and in which phases, are the metals redeposited? (3) What fraction of the mobilized metals is redeposited? (4) Does the concentration of metals in the fluid exceed drinking water guidelines?

2. Methods

2.1. Sampling and Analytical Methods

[12] Profiles from bleached to unbleached sandstones were cored using an electric diamond-edged 40 mm core plug drill, with samples spaced at 2–15 cm intervals. Samples near to the bleached-red contact were subsampled every 4 mm using a 2 mm tungsten-carbide drill bit. Between drilling, the bit and core were cleaned with compressed air. Samples were dissolved in HF and HNO_3 using an open beaker method, and analyzed by inductively coupled plasma (ICP)-atomic emission spectroscopy (major elements) and ICP-mass spectrometry (trace elements) in Cambridge, UK.

2.2. Mass of Metals in Enriched Zones

[13] The mass of a metal in the enriched region is determined by integrating across the enriched zone, assuming a stepped concentration profile. Uncertainties are estimated by propagating the uncertainties on the background and enriched compositions. The background compositions are taken as the average within the bleached zone (bleached sandstone), and the average composition of red sandstone near to the bleached fracture (unaltered sandstone; 1σ uncertainty; Table S1). The uncertainty in peak height is propagated 1σ instrument uncertainty, 1σ of repeat analyses, and recovery relative to USGS standard Sco-1 (Table S2). The range in the fraction of each metal redeposited is calculated from a Monte-Carlo simulation (n =1000) where each parameter listed above is allowed to vary within its range in uncertainty, and the range is given by 1σ about the mean of the resulting distribution.

2.3. Sequential Extraction

[14] The nature of the minerals hosting the redeposited metals was determined by a sequential extraction procedure (modified from *Tessier et al.*, 1979 and *Förstner*, 1982) applied to a selection of unaltered and bleached samples and to metal-enriched samples from subhorizontal reaction fronts. Leaching was performed at room temperature in five steps: (1) Water rinse: 1.5 mL deionized 18.2 MΩ water with continuous agitation for 2 h. (2) Exchangeable fraction: 1.5 mL 1 M sodium acetate solution (NaOAc) at pH 8.2, with continuous agitation for 3 h. (3) Carbonates: 1.5 mL 1 M NaOAc adjusted to pH 5 with acetic acid (HOAc), with continuous agitation for 7 h, repeated three times. (4) Oxides: 1.5 mL 0.1 M oxalate buffer adjusted to pH 3 with oxalic acid. Occasional agitation for 54 h, repeated three times. (5) HCl rinse (remaining carbonate/oxides): 1.5 mL 16 M HCl with continuous agitation for 2.5 h.

[15] After each leach, the sample was centrifuged for 30 min at 3000 rpm, and the liquid pipetted carefully into a cleaned centrifuge tube. The sample was then rinsed with 18.2 MΩ water, recentrifuged, and the rinse added to the leachate solution. After the final leaching step, the residue was dried down and dissolved in a combination of HF and HNO_3 in an open beaker method. The leachate solutions were evaporated to dryness and redissolved in a dilute nitric acid solution.

[16] The number of moles of a mineral phase dissolved in each sequential leaching step was

Table 1. Fraction of Each Mineral Released in Sequential Leaching Steps[a]

	Average Fraction Released				
	18.2 MΩ Water Rinse	Exchangeable Leach	Carbonate Leach	Oxide Leach	HCl Leach
Quartz	0.00 (0)	0.02 (1)	0.00 (0)	0.03 (1)	0.00 (0)
K-feldspar	0.10 (2)	0.17 (6)	0.01 (1)	0.12 (5)	0.01 (1)
Plagioclase	0.00 (0)	0.00 (0)	0.00 (0)	0.00 (0)	0.01 (0)
Clay	0.07 (1)	0.19 (7)	0.01 (0)	0.34 (12)	0.04 (1)
Calcite	0.04 (1)	0.23 (8)	0.63 (5)	0.00 (0)	0.84 (24)
Dolomite	0.05 (1)	0.05 (2)	0.18 (1)	0.17 (6)	0.04 (1)
Fe-dolomite	0.00 (0)	0.01 (0)	0.14 (1)	0.00 (0)	0.00 (0)
Hematite	0.00 (0)	0.00 (0)	0.01 (0)	0.29 (11)	0.06 (2)
Pyrite	0.00 (0)	0.00 (0)	0.00 (0)	0.04 (2)	0.00 (0)
Gypsum	0.73 (12)	0.34 (13)	0.02 (0)	0.00 (0)	0.00 (0)
TiO_2	0.00 (0)	0.00 (0)	0.00 (0)	0.00 (0)	0.00 (0)

[a]Numbers in parentheses are 1σ uncertainties for the last digit, calculated from the magnitude of the misfit to bulk rock values.

determined by a modal decomposition of the compositions of the leachate solutions. This was done by minimizing the difference between theoretical and observed compositions by varying the moles of each mineral dissolved. Mineral compositions of plagioclase, K-feldspar, and carbonates are taken from electron microprobe analyses (Table S5). An average clay composition is used based on the major element chemistry of the < 2μm fraction ($Al_{1.4}Ca_{0.2}Fe_{0.5}K_{0.8}Mg_{0.1}Na_{0.2}Si_{3.8}O_{10}(OH)_2$; recalculated to a 12 oxygen formula). Fe and Ti-oxides, pyrite and quartz are assumed to exist as pure phases.

3. Results and Discussion

3.1. Phases Dissolved During Sequential Extraction

[17] The results of the modal decomposition of sequential leaching solutions are shown in Table 1. The water rinse predominantly dissolves soluble salts, releasing up to 86% of available S with a Ca/S ratio of ≈1. Modal analysis on water rinse solutions shows that 75% of all minerals dissolved in this step are gypsum (Table 1). The exchangeable leach removes residual soluble salts and minor amounts of calcite and silicates. It also removes loosely adsorbed cations: in some samples, up to 60% of total Sr is removed in this step. Up to 80% total Ca and 60% total Mg are removed in the carbonate leach indicating dissolution of calcite and dolomite. Approximately 95% of minerals dissolved are carbonates. The oxide leach removes up to 60% of total Fe with a greater fraction released in bleached samples, reflecting the dissolution of secondary coarse oxide phases rather than grain coating oxy-hydroxides. Approximately 30% of the minerals dissolved are Fe-oxides, along with some clays and residual dolomite. A moderate correlation (R^2 =0.34) between Fe and S suggests dissolution of minor pyrite; however, an Fe/S ratio of ≈100 precludes pyrite dissolution as the dominant control on the Fe content of the leachate solution. The hydrochloric acid leach dissolves residual carbonate and oxide phases, and minor silicates. A larger fraction of total Fe is released in unaltered samples in this step, reflecting partial dissolution of the grain coating oxy-hydroxide phases.

3.1.1. Location of Redeposited Metals

[18] The results of the sequential extraction experiments are typified by cobalt (Co; Figure 5). In both bleached and unbleached samples where no enrichment is observed, Co is released from carbonate, oxides, and by dissolution of the residue (Figure 5a), indicating an equal distribution between carbonate, coarse oxides, and grain-coating phases. In samples with bulk rock Co enrichment, the Co released in the steps dissolving carbonate and oxide phases is two orders of magnitude greater than background values (Figure 5b). Redeposited trace metals are therefore incorporated into the secondary oxides and carbonates growing at the bleaching reaction front [*Wigley et al.*, 2012].

3.2. Fraction of Mobilized Metals Redeposited

[19] The minimum fraction of each trace metal redeposited can be calculated from bleached halos surrounding fractures where the displacement distance of the reaction front is given by the perpendicular distance of the front from the fracture.

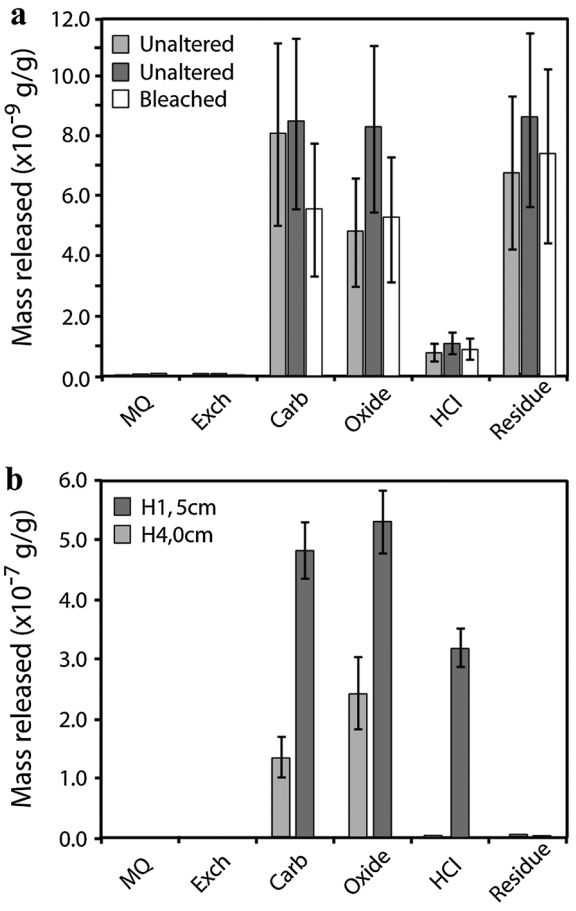

Figure 5. Results of sequential leaching for Co. (a) Mass of Co released in three samples without metal enrichment: two samples of unaltered sandstone and one sample of bleached sandstone 50 cm below the reaction front. Co is widely distributed between phases. (b) Mass of Co released in each leaching step for two samples which show enrichment in Co. Transect name, and distance from the red-bleached transition are given (positive numbers indicate unaltered rock). Note the different scales on the two graphs. Error bars are 2σ propagated recoveries relative to bulk rock concentrations and instrument uncertainties. Major and trace element composition of leaches are given in Table S6.

The theoretical mass of a metal mobilized along a one-dimensional path is given by the difference between the background concentrations in the red and bleached sandstones, and the displacement distance. The ratio of the predicted to observed mass of metal in the enriched zone gives a measure of the fraction of that metal redeposited at the reaction front.

[20] Some metals analyzed (Cu, V1; Zn, V2 and V3) exhibit redeposited fractions close to unity, with the adsorbed mass being within error of the total mass dissolved (Table 2). Others (Cu, V2 and V3; Co, V1) show enrichment relative to the mass dissolved by propagation of the reaction front from the fracture. The true value lies in the upper range of calculated results as the sampling may have missed peaks in concentration, thus underestimating the mass of metal that has been redeposited. Fluids entering the fractures have previously reacted with unaltered rock and may therefore be enriched in metals and these, along with metals mobilized by the reaction front moving away from the fracture, are all redeposited.

[21] Metals in solution exist either as free-metal cations or metal-anion complexes (e.g., with OH^-, HCO_3^-, or Cl^-). Speciation modeling using the geochemical speciation program PHREEQC [*Parkhurst and Appelo*, 1999] with the Lawrence Livermore National Laboratory database [*Johnson et al.*, 2000], using the calculated range in P_{CO_2} and salinity and assuming equilibrium with calcite, suggests that Sn, Zn, and Co exist as uncomplexed species, with a minor fraction of Co and Zn complexing with chloride and Zn also forming carbonate complexes (Figure S2); Cu speciation is dominated by chloride species. Realistic variations in methane concentrations do not significantly change metal speciation profiles. This shows that metal complexation does not play a major role in the redeposition process, as metals complexing with hydroxyl, carbonate, and chloride anions as well as free metal cations are all redeposited at the CO_2-promoted reaction fronts.

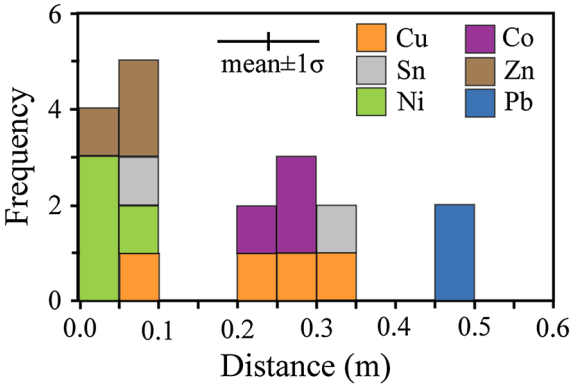

Figure 6. Calculated vertical distances moved by the subhorizontal bleaching reaction front. Colors represent calculations of different metal enrichments. Uncertainties are 1σ of background uncertainties in red and bleached sandstone propagated with peak height uncertainties.

Table 2. Enrichment Factors, Fractions of Each Metal Redeposited, TIFF, and Calculated Fluid Concentrations for the Fracture-Associated Bleaching Reaction Fronts[a]

Metal	Transect	Advective Distance (m)	Enrichment Factor	Fraction Redeposited	TIFF (m^2/m^3)	Enriched Zone Width (m)	Av. Fluid Concentration (mg/L)
Cu	V1	0.51	18 (1)	0.6 (4)	13.0	0.006	0.117
	V2	0.08	20 (5)	2.8 (20)	2.0	0.01	0.342
	V3	0.07	7 (2)	3.4 (24)	1.7	0.006	0.579
Zn	V2	0.08	8 (3)	0.9 (5)	2.0	0.008	0.294
	V3	0.07	3 (1)	1.3 (8)	1.7	0.008	0.436
Co	V1	0.51	21 (1)	2.8 (17)	13.0	0.006	0.029
Sn	V1	0.51	12 (3)	0.4 (3)	13.0	0.006	0.007

[a]Numbers in parentheses are 1σ uncertainties on the last digit. Uncertainties for fraction readsorbed and enrichments are 1σ of background uncertainties in red and bleached sandstone propagated with peak height uncertainties.

[22] Transport of mobilized metals is thus controlled by the distance moved by CO_2-promoted reaction fronts, rather than by the distance moved by the fluid. The difference between these length scales is controlled by the stoichiometry and kinetics of the fluid-rock reactions, and therefore the mineralogy of the host formation. In nonreactive reservoirs, mobilized metals will be transported further; however, such reservoirs are less likely to contain significant quantities of contaminants.

3.3. Vertical Transport Distances Across Subhorizontal Reaction Fronts

[23] The observation that the metals removed from the bleached sandstone are quantitatively redeposited can be used to calculate transport distances perpendicular to the subhorizontal reaction fronts. The length of rock bleached by the fluid interacting with horizontal reaction fronts is calculated using the difference in background concentration in bleached and unbleached samples and the mass of each metal deposited at the reaction front, assuming 100% redeposition ($l = M/\Delta C$; where l is the length of rock bleached (m), M is the mass of the metal in the enrichment (mol m^{-2}), and ΔC (mol m^{-3}) is the difference in background concentrations between red and bleached sandstone). Some metals may have been removed by the subhorizontal advection of the gravity current although this flux may decrease near the margin of a gravity current. If so the calculation underestimates the transport distance. Four transects across horizontal reaction fronts were analyzed (H1–4), and the length of rock bleached for each unit area of reaction front is low (<0.35 m; Figure 6), consistent with the CO_2-rich brine migrating as a gravity current with vertical motion dominated by diffusive processes except near open fractures.

3.4. Potential Impact on Water Quality

[24] The enrichment of metals in the fluid is calculated from the mass of metal deposited at the reaction front and the volume of fluid required to transport this mass. The time integrated fluid flux (TIFF, the volume of fluid that has interacted with the reaction front) is calculated from the retardation factor (R) and the distance the front is displaced (Table 2). R is defined as the volume of fluid required to displace the reaction front through a unit volume of rock, and is estimated from the reaction stoichiometry and change in brine-CO_2 concentration across the reaction front. TIFF is then given by R × distance, i.e., the volume of fluid required to displace the reaction front through the observed volume of rock.

[25] Metal concentrations in the fluid (C_m; mol m^{-3}) as the reaction front propagates are given by the following:

$$C_m = \frac{F_m}{F_f} \quad (1)$$

where F_m is the metal flux (mol m^{-2} s^{-1}), and F_f is the fluid flux (m s^{-1}). The time-averaged metal flux is given by the mass of metal in the enrichment (mol/m^2 reaction front); and the TIFF is the corresponding F_f (m^3/m^2; Table 2).

[26] Calculated concentrations of Cu and Zn are an order of magnitude below the World Health Organization (WHO) drinking water limit (Cu: 2 mg/L, Zn: 5 mg/L) [*WHO*, 2011], and Sn concentrations are well below acceptable limits (150 mg/L) [*WHO*, 2003]. No guidelines exist for Co; however, calculated Co concentrations are 10 times the average composition of U.S. freshwater [*ATSDR*, 2004] (a worked example is presented in Appendix A).

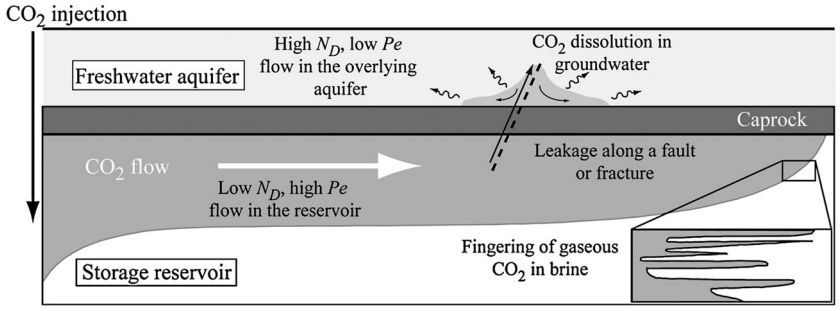

Figure 7. Schematic description of a CO_2 injection site. If CO_2 migrates into overlying groundwater systems with low natural fluid flow rates, then conditions may be similar to those in the Green River analogue site where the low transport rates mean that reaction fronts retard the potential transport of metals.

4. Concluding Remarks

[27] The reaction fronts studied here, where fluid velocities are low and diffusive processes are important, have a high Damköhler number (N_D; the ratio of reaction rate to rate of advection) and a low Peclet number (Pe; the ratio of advective to diffusive transport). The high injection pressures in CO_2-storage reservoirs will result in high rates of advection, and consequently CO_2-promoted reaction fronts will have a lower N_D and a higher Pe than those documented here. However, much of the concern over contaminant mobilization relates to migration of CO_2 into overlying aquifers where the groundwater flow rates are likely to be considerably lower (Figure 7), being dominated by regional gradients in hydraulic head, such that reaction fronts have a transport characteristic comparable to those studied here. In this context, our results show that mobilized metals are redeposited over small length scales in secondary phases precipitating at the CO_2-promoted reaction fronts. Fundamentally, this redeposition process is thought to be driven by buffering of pH by fluid-rock reactions at the reaction front, although a full reactive-transport description of the system is required to fully evaluate the redeposition process. Fluxes of CO_2-charged waters of approximately 25 times the volume of an aquifer of the composition of the Entrada sandstone would be required for reaction fronts to pass through the aquifer and for mobile trace metals to be extracted.

Acknowledgments

[28] MW would like to thank Jason Day for advice with sequential leaching and geochemical analyses. Carbon research at Cambridge is supported by Natural Environment Research Council grant NE/F004699/1, part of the UK CRIUS (Carbon Research into Underground Storage) consortium. Niko Kampman is a recipient of financial support from Shell International. The manuscript was significantly improved as a result of comments by two anonymous reviewers.

Appendix A: Calculating Metal Concentrations in the Fluid: A Worked Example

[29] Calculation of the concentration of a metal in the fluid leaving the reaction front requires an estimate of the retardation factor of the formation and knowledge of the distance moved by the reaction front and the mass of the metal under consideration deposited at the reaction front.

[30] The retardation factor, R, is given by the following:

$$R = \frac{M_{hem}.S}{\Delta CO_2} \quad (A1)$$

where M_{hem} is the number of moles of hematite per m^3 formation ($\approx$40 moles/m^3), S is the number of moles of CO_2 needed to dissolve 1 mole of hematite ($\approx$3.2) [*Wigley et al.*, 2012], and ΔCO_2 is the change in CO_2 concentration in the fluid across the reaction front ($\approx$5 mol/m^3) [*Wigley et al.*, 2012]. This gives a retardation factor of approximately 25.6.

[31] The metal concentration is given by the metal flux divided by the fluid flux (equation (1)). By integrating over the duration of the bleaching event, this reduces to the following:

$$\text{Concentration} = \frac{M}{\text{TIFF}} \quad (A2)$$

where M is the mass of metal at the reaction front (kg/m^2) and TIFF is the time integrated fluid flux (m^3/m^2), which is given by: R×X, where X is the distance moved by the reaction front (m).

[32] The mass of copper deposited at reaction front V1 is 0.00152 kg/m^2, and the reaction front has moved 0.506 m. The corresponding TIFF is therefore 13 m^3/m^2, and the concentration of copper in the fluid as the reaction front propagates is 0.000117 kg/m^3 or 0.117 mg/L.

References

Agency for Toxic Substances and Disease Registry (2004), *Toxicological Profile for Cobalt*, Department of Health and Human Services, Public Health Service, Atlanta, GA.

Assayag, N., M. Bickle, N. Kampman, and J. Becker (2009), Carbon isotopic constraints on CO_2 degassing in cold-water geysers, Green River, Utah, *Energy Procedia*, *1*(1), 2361–2366, doi:10.1016/j.egypro.2009.01.307. Greenhouse Gas Control Technologies 9: Proceedings of the 9th International Conference on Greenhouse Gas Control Technologies (GHGT-9), 20 November 2008, Washington DC, USA.

Beitler, B., M. A. Chan, and W. T. Parry (2003), Bleaching of Jurassic Navajo sandstone on Colorado Plateau laramide highs: Evidence of exhumed hydrocarbon supergiants? *Geology*, *31*(12), 1041–1044, doi:10.1130/G19794.1.

Beitler, B., W. Parry, and M. A. Chan (2005), Fingerprints of fluid flow: Chemical diagenetic history of the Jurassic Navajo Sandstone, Southern Utah, U.S.A., *J. Sediment. Res.*, *75*(4), 547–561, doi:10.2110/jsr.2005.045.

Benjamin, M. M., and J. O. Leckie (1981), Multiple-site adsorption of Cd, Cu, Zn, and Pb on amorphous iron oxyhydroxide, *J. Colloid Interface Sci.*, *79* (1), 209–221, doi:10.1016/0021-9797(81)90063-1.

Bickle, M. J. (2009), Geological carbon storage, *Nat. Geosci.*, *2*(12), 815–818, doi:10.1038/ngeo687.

Bickle, M. J., and J. Baker (1990), Advective-diffusive transport of isotopic fronts: An example from Naxos, Greece, *Earth Planet. Sci. Lett.*, *97*(12), 78–93, doi:10.1016/0012-821X(90)90100-C.

Bradl, H. B. (2004), Adsorption of heavy metal ions on soils and soils constituents, *J. Colloid Interface Sci.*, *277*(1), 1–18, doi:10.1016/j.jcis.2004.04.005.

Chan, M. A., W. Parry, and J. R. Bowman (2000), Diagenetic hematite and manganese oxides and fault-related fluid flow in Jurassic Sandstones, Southeastern Utah, *AAPG Bull.*, *84*(9),1281–1310, doi:10.1306/A9673E82-1738-11D7-8645000102C1865D.

Cullers, R. L. (1995), The controls on the major- and trace-element evolution of shales, siltstones and sandstones of Ordovician to tertiary age in the Wet Mountains Region, Colorado, U.S.A., *Chem. Geol.*, *123*(1-4), 107–131, doi:10.1016/0009-2541(95)00050-V.

Dockrill, B., and Z. K. Shipton (2010), Structural controls on leakage from a natural CO_2 geologic storage site: Central Utah, U.S.A., *J. Struct. Geol.*, *32*(11), 1768–1782, doi:10.1016/j.jsg.2010.01.007.

Duan, Z., R. Sun, C. Zhu, and I. Chou (2006), An improved model for the calculation of CO_2 solubility in aqueous solutions containing Na^+, K^+, Ca^{+2}, Mg^{+2}, Cl^-, and SO_4^{+2}, *Mar. Chem.*, *2-4*, 131–139, doi:10.1016/j.marchem.2005.09.001.

Dubacq, B., M. Bickle, M. Wigley, N. Kampman, C. Ballentine, and Sherwood-Lollar B. (2012), Noble gas and carbon isotopic evidence for CO_2-driven silicate dissolution in a recent natural CO_2 field, *Earth Planet. Sci. Lett.*, *341-344*, 10–19, doi:10.1016/j.epsl.2012.05.040.

Förstner, U. (1982), Accumulative phases for heavy metals in limnic sediments, *Hydrobiologia*, *91-92*, 269–284, doi:10.1007/BF02391944.

Gale, J. (2004), Geological storage of CO_2: What do we know, where are the gaps and what more needs to be done?, *Energy*, *29*(9-10), 1329–1338, doi:10.1016/j.energy.2004.03.068.

Garden, I. R., S. C. Guscott, S. D. Burley, K. A. Foxford, J. J. Walsh, and J. Marshall (2001), An exhumed palaeohydrocarbon migration fairway in a faulted carrier system, Entrada Sandstone of SE Utah, USA, *Geofluids*, *1*(3), 195–213, doi:10.1046/j.1468-8123.2001.00018.X.

Intergovernmental Panel on Climate Change, (2007), Fourth assessment report: Climate change 2007: Working group I report: The physical science basis, IPCC, Geneva.

Johnson, J., G. Anderson, and D. Parkhurst (2000), Database 'thermo.com.v8.r6.230', Rev. 1.11, Lawrence Livermore Natl. Lab., Livermore, California.

Kampman, N., M. Bickle, J. Becker, N. Assayag, and H. Chapman (2009), Feldspar dissolution kinetics and Gibbs free energy dependence in a CO_2-enriched groundwater system, Green River, Utah, *Earth Planet. Sci. Lett.*, *284*(34), 473–488, doi:10.1016/j.epsl.2009.05.013.

Kampman, N., N. M. Burnside, Z. K. Shipton, H. J. Chapman, J. A. Nicholl, R. M. Ellam, and M. J. Bickle (2012), Pulses of carbon dioxide emissions from intracrustal faults following climatic warming, *Nat. Geosci.*, *5*, 352–358, doi:10.1038/ngeo1451.

Keating, E., J. Fessenden, N. Kanjorski, D. Koning, and R. Pawar (2010), The impact of CO_2 on shallow groundwater chemistry: Observations at a natural analog site and implications for carbon sequestration, *Environ. Earth Sci.*, *60*, 521–536, doi:10.1007/s12665-009-0192-4.

Kharaka, Y., et al. (2010), Changes in the chemistry of shallow groundwater related to the 2008 injection of CO_2 at the ZERT Field Site, Bozeman, Montana, *Environ. Earth Sci.*, *60*, 273–284, doi:10.1007/s12665-009-0401-1.

Little, M. G., and R. B. Jackson (2010), Potential impacts of leakage from deep CO_2 geosequestration on overlying freshwater aquifers, *Environ. Sci. Technol.*, *44*(23), 9225–9232, doi:10.1021/es102235w.

Loope, D. B., R. M. Kettler, and K. A. Weber (2010), Follow the water: Connecting a CO_2 reservoir and bleached sandstone to iron-rich concretions in the Navajo Sandstone of South-Central Utah, USA, *Geology*, *38*(11), 999–1002, doi:10.1130/G31213.1.

Lu, J., J. Partin, S. Hovorka, and C. Wong (2010), Potential risks to freshwater resources as a result of leakage from CO_2 geological storage: A batch-reaction experiment, *Environ. Earth Sci.*, *60*, 335–348, doi:10.1007/s12665-009-0382-0.

Lu, W., I. Chou, R. C. Burruss, and Y. Song (2007), A unified equation for calculating methane vapor pressures in the CH_4-H_2O system with measured Raman shifts, *Geochim. Cosmochim. Acta*, *71*, 3969–3978, doi:10.1016/j.gca.2007.06.004.

Nuccio, V. F. (2000), Burial and thermal history of the Paradox Basin, Utah and Colorado, and petroleum potential of the Middle Pennsylvanian paradox formation, United States Geological Survey. United States Geological Survey bulletin, 2000-O.

Parkhurst, D. L., and C. A. J. Appelo, (1999), User's guide to PHREEQC (version 2) - A computer program for speciation, batch-reaction, one-dimensional transport, and inverse geochemical calculations, *(Water-Resources Investigations Report 99-4259)*.

Rosso, K., and R. Bodnar (1995), Microthermometric and Raman spectroscopic detection limits of CO_2 in fluid inclusions and the Raman spectroscopic characterization of CO_2, *Geochim. Cosmochim. Acta*, *59*(19), 3961–3975, doi:10.1016/0016-7037(95)94441-H.

World Health Organization, (2003), Hydrogen sulfide in drinking water. Background document for preparation of WHO guidelines for drinking water quality, *Report no. WHO/SDE/WSH/03.04/07*.

World Health Organization (2011), Guidelines for drinking-water quality. ISBN: 92 4 154696 4.

Smyth, R. C., S. D. Hovorka, J. Lu, K. D. Romanak, J. W. Partin, C. Wong, and C. Yang (2009), Assessing risk to fresh water resources from long term CO_2 injection-laboratory and field studies, *Energy Procedia*, *1*(1), 1957–1964, doi:10.1016/j.egypro.2009.01.255. Greenhouse Gas Control Technologies 9, Proceedings of the 9th International Conference on Greenhouse Gas Control Technologies (GHGT-9), 16-20 November 2008, Washington DC, USA.

Tessier, A., P. G. C. Campbell, and M. Bisson (1979), Sequential extraction procedure for the speciation of particulate trace metals, *Anal. Chem.*, *51*(7), 844–851, doi:10.1021/ac50043a017.

Trimble, L. (1978), *Geology and Uranium-Vanadium Deposits of the San Rafael River Mining Area, Emery County, Utah*, pp. 24–34, vol. 113, Utah Geological and Mineral Survey, Salt Lake City.

Wigley, M., N. Kampman, B. Dubacq, and M. Bickle (2012), Fluid-mineral reactions and trace metal mobilization in an exhumed natural CO_2 Reservoir, Green River, Utah, *Geology*, *40*, 555–558, doi:10.1130/G32946.1.

Wigley, M., B. Dubacq, N. Kampman, and M. Bickle (2013), Controls on sluggish, CO_2-promoted Hematite and K-feldspar dissolution kinetics in sandstones, *Earth Planet. Sci. Lett.*, *362*, 76–87, doi:10.1016/j.epsl.2012.11.045.

Wilkin, R. T., and D. C. DiGiulio (2010), Geochemical impacts to groundwater from geologic carbon sequestration: Controls on ph and inorganic carbon concentrations from reaction path and kinetic modeling, *Environ. Sci. Technol.*, *44*(12), 4821–4827, doi:10.1021/es100559j. pMID: 20469895.

Yin, Y., H. E. Allen, Y. Li, C. P. Huang, and P. F. Sanders (1996), Adsorption of mercury(II) by soil: Effects of pH, chloride, and organic matter, *J. Environ. Qual.*, *25*(4), 837–844, doi:10.2134/jeq1996.00472425002500040027x.

Zheng, L., J. A. Apps, Y. Zhang, T. Xu, and J. T. Birkholzer (2009), On mobilization of lead and arsenic in groundwater in response to CO_2 leakage from deep geological storage, *Chem. Geol.*, *268* (3-4), 281–297, doi:10.1016/j.chemgeo.2009.09.007.